Journal of Materials Science: Materials in Electronics (2019) 30:6201–6211
https://doi.org/10.1007/s10854-019-00922-z

Physico-chemical studies of $Cd_{1-x}Zn_xS$ thin films produced by simple two-electrode electrodeposition system for solar cell application

S. Z. Werta[1] · O. K. Echendu[1] · F. B. Dejene[1]

Received: 21 December 2018 / Accepted: 11 February 2019 / Published online: 15 February 2019

Abstract

$Cd_{1-x}Zn_xS$ thin films have been cathodically electrodeposited on glass/fluorine-doped tin oxide substrates using a low-cost two-electrode configuration with an electrolytic bath containing cadmium chloride, zinc chloride and sodium thiosulphate precursors. The deposition was carried out by varying zinc chloride concentration (0 M, 0.3 M, 0.6 M and 0.9 M) in the deposition electrolyte. The structural, compositional, phonon vibrational, morphological and optical properties of the resulting films have been characterized using glancing incidence X-ray diffraction, energy-dispersive X-ray (EDX) spectroscopy, Raman spectroscopy, scanning electron microscopy (SEM) and UV–Vis spectrophotometry respectively. The XRD result indicates the existence of hexagonal structure of $Cd_{1-x}Zn_xS$ with intensities of the diffraction peaks decreasing as more Zn is incorporated into the film as a result of decrease in deposition rate. EDX results show the presence of Cd, Zn and S in the deposited $Cd_{1-x}Zn_xS$ thin films. SEM images show uniform and densely packed surface morphology of the films with distinct shaped grains which gradually less distinct as more Zn is incorporated into the films. The optical measurements reveal a significant increase in energy band gap of the $Cd_{1-x}Zn_xS$ material as more zinc is incorporated into the films and a film thickness decreases with the energy band gap increasing from 2.40 eV for CdS to 2.62 eV for $Cd_{1-x}Zn_xS$. These results show that $Cd_{1-x}Zn_xS$ material can be applied as a better window material for CdTe, CIG(S,Se) and CZTS-based solar cells than CdS.

1 Introduction

CdS and ZnS are renowned wide and direct band gap group II–VI semiconductors with bulk band gaps, (E_g) of 2.42 eV and 3.68 eV respectively [1, 2]. These band gap values are convenient when these materials are used as n-type window materials in CdTe, CuIn(S,Se) and Cu(In,Ga)Se photovoltaic solar cells [3–7]. Despite the fact that, CdS and ZnS are popularly used as window materials and as n-type heterojunction partners to p-type absorber materials, CdS is known to have high coefficient of absorption while ZnS is highly resistive [8, 9]. To minimize the solar absorption loss associated with the high absorption coefficient of CdS and the high resistivity associated with ZnS, ternary alloyed compounds like $Cd_{1-x}Zn_xS$ have attracted research interest due to the fact that the energy band gap of such materials can be tuned and the lattice parameters can be varied [10, 11]. $Cd_{1-x}Zn_xS$ thin film has properties in between CdS and ZnS, and it is formed by substituting Zn for Cd in CdS lattice. The addition of Zn improves optical properties of $Cd_{1-x}Zn_xS$ thin film for solar cell application in such a way that it reduces the optical absorbance and increase the transmittance as compared to CdS. This helps to reduce the window absorption loss associated with CdS. Other than for photovoltaic solar cells as a window material, $Cd_{1-x}Zn_xS$ compound has also been used for different applications such as in water treatment, optical filters, gas sensors, multilayer light emitting diodes (LEDs), field effect transistors, and other optoelectronic devices [12–15].

Various techniques such as electrodeposition [16], chemical bath deposition [17], chemical vapour deposition [18], vacuum evaporation [19], co-precipitation [20], spray pyrolysis [21], sol–gel [22], metal organic chemical vapour deposition (MOCVD) [23], pulsed laser deposition (PLD) [24], RF sputtering [25], and close space sublimation (CSS) [26] have been employed for the synthesis of $Cd_{1-x}Zn_xS$ thin films. Though, $Cd_{1-x}Zn_xS$ thin film can be deposited using these listed deposition techniques, using electrodeposition method has not been investigated adequately in order to explore the advantages of electrodeposition technique which

✉ S. Z. Werta
solomonwerta@gmail.com

[1] Department of Physics, University of the Free State, Qwa Qwa Campus, Private bag X13, Phuthaditjhaba 9866, South Africa

include large area deposition, long bath lifetime, minimum waste generation, easy process control, and self-purification of electrolytic bath [27–29]. Hence in this paper electrodeposition technique has been used as a viable technique to obtain quality $Cd_{1-x}Zn_xS$ thin films. Typically, in the deposition of thin films using electrodeposition technique, the use of reference electrode is common. But nowadays, two electrode configuration has become promising by reducing the cost due to the reference electrode and avoiding possible contamination of the electrolytic solution in the case of reference electrode with leaky or broken frit [29, 30]. For these reasons, and the fact that small variations in deposition voltage does not have significant influence in the case of semiconductor deposition at least [29], a simple two-electrode deposition set-up is used in the present work. In electrodeposition technique, optimization of deposition conditions, such as electrolytic bath temperature, deposition time, pH, stirring, electrodes used, concentration of ions in the electrolytic bath and applied voltage, is essential to improve the physico-chemical properties of deposited films [27, 28]. Hence, by careful choice of these deposition conditions, in this paper, the influence of Zn concentration on the physico-chemical properties of $Cd_{1-x}Zn_xS$ thin films investigated using a simple two-electrode deposition configuration for possible solar cell application. This approach has not been reported yet.

2 Experimental details

$Cd_{1-x}Zn_xS$ thin films were cathodically electrodeposited from aqueous electrolytic solution containing 0.3 M of cadmium chloride ($CdCl_2$), as Cd source, different concentrations (0 M, 0.3 M, 0.6 M, and 0.9 M) of zinc chloride ($ZnCl_2$), as zinc source and 0.03 M sodium thiosulphate ($Na_2S_2O_3$) as sulphur source in 400 ml of deionised water. All the chemicals were laboratory reagent grade purchased from Sigma-Aldrich. Fluorine-doped thin oxide coated glass (glass/FTO) substrates were used for the deposition. All glass/FTO substrates were immersed in a diluted laboratory soap solution and cleaned ultrasonically for 30 min. Thereafter, these substrates were washed using acetone, ethanol and methanol while rinsing with de-ionized water in between washing, and finally dried in air. Figure 1 shows a schematic of the low-cost two-electrode deposition set-up, which was also used to carry out a cyclic voltammetry (CV) of the deposition electrolyte. For CV measurement and deposition of the films, a computerized Gill AC potentiostat (ACM instruments, United Kingdom) and high-purity graphite rod as counter electrode, have been used, with glass/FTO substrate as working electrode. Due to the fact that, $S_2O_3^{2-}$ dissociates at relatively lower cathodic potential, sulphur comes to deposit first on the substrate from around cathodic potential

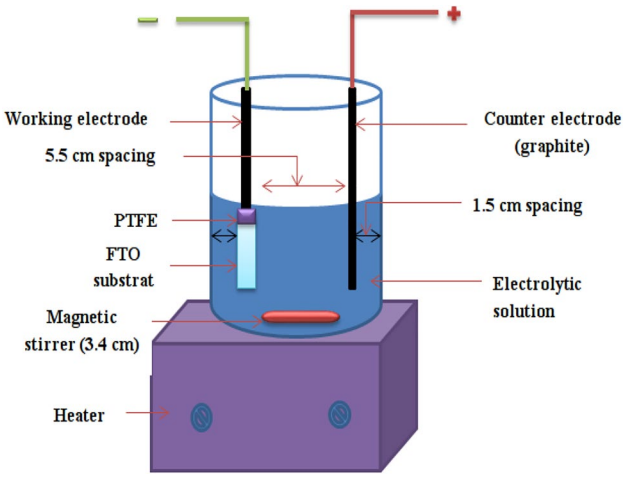

Fig. 1 Simplified 2-electrode electrodeposition set-up used for growing $Cd_{1-x}Zn_xS$

of 400 mV and the current density is low. As seen in Fig. 2, as cathodic potential increases in the region between 1400 and 1600 mV, both sulphur and cadmium begin to co-deposit and a gradual increase in current density is observed. But, as the cathodic potential goes above 1600 up to 1900 mV, despite the fact that Zn^{2+} has relatively higher standard reduction potential of −760 mV than Cd^{2+} (−403 mV) and $S_2O_3^{2-}$, all sulphur, cadmium and zinc start to co-deposit and sharp increase in current density is observed in the cyclic voltammetry graph. The reaction mechanisms for the formation of CdS and CdZnS are presented as shown in Eqs. (1–3) starting with the dissociation of the thiosulphate ions in the presence of acid in the electrolyte. Hence, the possible cathodic deposition voltages for $Cd_{1-x}Zn_xS$ were found from the cyclic voltammogram to be between 1600 and 1900 mV. In-between these two voltages different preliminary depositions were done and −1700 mV was settled for as the best deposition potential.

$$S_2O_3^{2-} + 6H^+ + 6e^- \rightarrow 3H_2O + S^{2-} + S(s) \quad (1)$$

Then for formation of CdS on the cathode, we have

$$Cd^{2+} + S^{2-} \rightarrow CdS \quad (2)$$

And for the formation of CdZnS, we have

$$Cd^{2+} + Zn^{2+} + S^{2-} + 2e^- \rightarrow CdZnS \quad (3)$$

pH of the electrolytic bath was settled at 3.5 ± 0.02, and dilute hydrochloric acid (HCl) and ammonium hydroxide (NH_4OH) were used to control the pH. Moderate stirring rate of the electrolytic bath with a bath temperature of 85 °C and deposition time 30 min. were applied. Following this, the deposition of $Cd_{1-x}Zn_xS$ thin films was carried out using four pre-cleaned glass/FTO substrates at four different zinc chloride concentrations of 0 M, 0.3 M, 0.6 M and

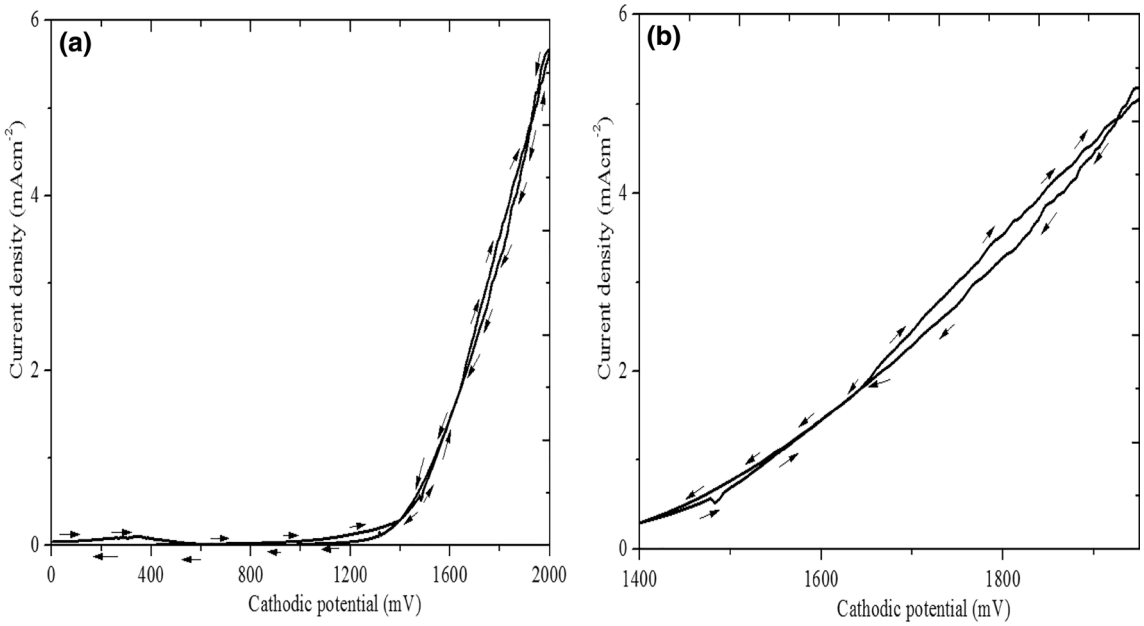

Fig. 2 **a** Simplified 2-electrode cyclic voltammogram of 0.3 M $CdCl_2$, 0.3 M $ZnCl_2$ and 0.03 M $Na_2S_2O_3$ for deposition of $Cd_{1-x}Zn_xS$ thin films. **b** Expanded view of $Cd_{1-x}Zn_xS$ deposition potential range

0.9 M $ZnCl_2$ with steps of 0.3 M in-between. Afterwards, all electrodeposited $Cd_{1-x}Zn_xS$ thin film samples were rinsed with de-ionized water and then dried in air. Finally, all electrodeposited $Cd_{1-x}Zn_xS$ thin films were annealed at 400 °C for 20 min for physical and chemical characterization. Hence, all the data reported in this paper are for the annealed samples since this is the best form of the materials for solar cell application.

For characterization, glancing incidence X-ray diffraction (GIXRD) was carried out using Rigaku Smartlab X-ray diffractometer (Rigaku Corporation, USA); scanning electron microscopy (SEM) was carried out using Tescan VEGA3 SEM machine (Tescan Corporation, Czech Republic); energy-dispersive X-ray (EDX) was carried out using the SEM machine with Oxford X-Max^N EDS detector attached to it; Raman spectroscopy was carried out using the alpha 300 R Confocal Raman machine (WITec, Germany) and UV–Vis spectrophotometry was carried out using a Shimadzu UV-1700PC spectrophotometer (Shimadzu, Corporation, Kyoto, Japan).

3 Results and discussion

3.1 Structural properties

X-ray diffraction measurements were carried out using glancing incidence X-ray diffraction (GIXRD) to study crystal structure and crystalline quality of the deposited $Cd_{1-x}Zn_xS$ thin films. It is known that, $Cd_{1-x}Zn_xS$ thin films can exist in cubic, hexagonal or mixed phase crystal structure based on preparation condition [1, 31, 32]. As shown in Fig. 3, the XRD patterns show the presence of only hexagonal phase peaks at all the different $ZnCl_2$ concentrations used. These peaks occur at diffraction angles of $2\theta = 24.92°$, 26.56°, 28.22°, 43.84° and 48.04° corresponding to diffraction lattice planes of (100)H, (002)H, (101)H, (110)H and (103)H respectively as can be seen in the patterns of all the samples. These diffraction peaks of the samples compare very well with those of Joint Committee

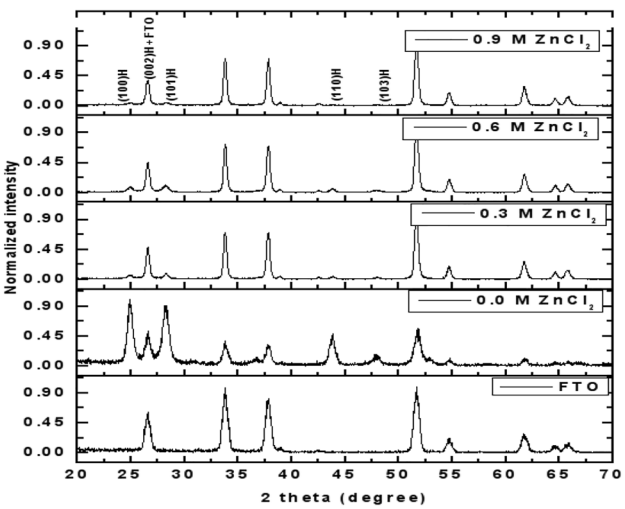

Fig. 3 GIXRD patterns of annealed $Cd_{1-x}Zn_xS$ thin films grown at zinc chloride concentrations

on Powder Diffraction and Standards (JCPDS) reference files 00-049-1302 for hexagonal CdZnS. Likewise, for pure CdS thin film (with 0 M $ZnCl_2$) hexagonal CdS phase peaks are also observed at diffraction angles of 2θ = 24.89°, 26.62°, 28.24°, 43.84° and 47.70° corresponding to diffraction lattice planes of (100)H, (002)H, (101)H, (110)H and (103)H respectively which match JCPDS reference file 01-080-0006 for hexagonal CdS.

As can be seen from Fig. 3, at 0 M $ZnCl_2$ concentration, the film (CdS) is very crystalline and even the FTO peaks are dwarfed by the high intensities of CdS peaks. But, as Zn is incorporated into CdS lattice, intensities of the major XRD peaks of $Cd_{1-x}Zn_xS$ [i.e. (100) and (101) peaks] start to decrease in relation to the FTO peaks. This decrease in intensity of $Cd_{1-x}Zn_xS$ thin film peaks, which also correspond with those of CdS, continues up to 0.6 M $ZnCl_2$. At 0.9 M $ZnCl_2$ the intensities of the XRD peaks are diminished considerably. It is known that, in electrodeposition technique ions are brought to the surface of the substrate by migration, convection and drift. Hence, when more $ZnCl_2$ is added into the electrolytic solution the concentration of Zn ions in the bath will increase and this increases the possibility of more zinc getting incorporated into CdS lattice to form $Cd_{1-x}Zn_xS$ thin films. In addition, the presence of more Zn^{2+} in the electrolyte results in low deposition rate of CdZnS as will be seen later from the calculated deposition rates in Table 2. Therefore, a decrease in intensity of the peaks may happen largely due to reduced thickness of the resulting CdZnS films as a result of low deposition rate.

The crystallite sizes (D), from Scherrer formula, the interplanar spacings (d_{hkl}), from Bragg's diffraction equation and lattice constants (a,b,c), using the formula for a hexagonal system, are calculated using Eqs. (4–6).

$$D = \frac{0.94\lambda}{\beta \cos\theta} \tag{4}$$

$$d_{hkl} = \frac{n\lambda}{2\sin\theta} \tag{5}$$

$$\frac{1}{d^2} = \frac{4}{3}\left(\frac{h^2 + hk + k^2}{a^2}\right) + \frac{l^2}{c^2} \tag{6}$$

where λ is X-ray wavelength, which is 1.54 Å, β is full width at half maximum (FWHM) of the diffraction peaks, θ is the diffraction angle, n is an integer and (hkl) are Miller indices from the JCPDS reference files. The lattice constants, $a = b$ are obtained from the plane (100), while the plane (002) is used to obtain the lattice constant c.

Summary of the structural parameters obtained from the XRD results for all annealed $Cd_{1-x}Zn_xS$ samples grown with the different zinc chloride concentrations is presented in Table 1.

Values in brackets are standard values for the reference material. (Lattice parameters from JCPDS reference file

Table 1 Lattice parameters obtained from XRD measurements

$ZnCl_2$ Concentration (M)	2θ (°)	*h k l*	d-Spacing (Å)	β (°)	D (nm)	D_{av} (nm)
0	24.89 (24.92)	(100)H	3.50 (3.56)	0.68	21.7	
	26.62 (26.66)	(002)H	3.34 (3.34)	0.60	24.9	
	28.24 (28.32)	(101)H	3.20 (3.14)	0.74	20.2	22.1
	43.84 (43.90)	(110)H	2.08 (2.06)	0.62	25.1	
	47.70 (48.11)	(103)H	1.92 (1.88)	0.74	21.5	
0.3	24.92 (24.83)	(100)H	3.50 (3.58)	0.60	24.6	
	26.56 (26.52)	(002)H	3.34 (3.35)	0.38	39.2	
	28.16 (28.20)	(101)H	3.20 (3.16)	0.64	23.3	24.0
	43.90 (43.73)	(110)H	2.08 (2.06)	0.54	28.8	
	47.90 (47.87)	(103)H	1.87 (1.89)	0.82	19.4	
0.6	24.92 (24.83)	(100)H	3.50 (3.58)	0.66	22.4	
	26.56 (26.52)	(002)H	3.34 (3.35)	0.38	39.2	
	28.22 (28.20)	(101)H	3.20 (3.16)	0.64	23.3	22.2
	43.84 (43.73)	(110)H	2.08 (2.06)	0.56	27.8	
	48.04 (47.87)	(103)H	1.87 (1.89)	1.02	15.6	
0.9	24.90 (24.83)	(100)H	3.50 (3.58)	0.66	5.50	
	26.60 (26.52)	(002)H	3.34 (3.35)	0.38	39.2	
	28.26 (28.20)	(101)H	3.20 (3.16)	1.22	12.2	10.8
	43.88 (43.73)	(110)H	2.05 (2.06)	1.34	11.6	
	48.04 (47.92)	(103)H	1.88 (1.89)	1.16	13.7	

00-049-1302 are a = b = 4.13 Å and c = 6.71 Å and the calculated values are a = b = 4.03 and c = 6.69 Å. For JCPDS file 01-080-0006: a = b = 4.12 and c = 6.68 Å and calculated values are a = b = 4.03 and c = 6.69 Å).

As shown in the Table 1, the values of FWHM and the corresponding crystallite sizes change as $ZnCl_2$ concentration increases in the electrolytic bath. The average crystallite size (D_{av}) was calculated for each $ZnCl_2$ concentration and it ranges from 24.0 to 10.8 nm as $ZnCl_2$ concentration increases. With no $ZnCl_2$ in the bath, D_{av} is 22.1 nm. With 0.3 M $ZnCl_2$ in the solution the average crystallite size increases to 24.0 nm. However, as more $ZnCl_2$ (0.6 M and 0.9 M) is added into the solution the average crystallite size decreases successively to 22.2 nm and 10.7 nm respectively. This decrease in average crystallite size reflects deterioration of crystallinity of $Cd_{1-x}Zn_xS$ thin films as more Zn is incorporated into the film as a result of decrease in deposition rate of the films as will be seen later.

3.2 Compositional characterization

EDX measurements have been taken to confirm the composition of the $Cd_{1-x}Zn_xS$ thin films. Figure 4 shows two representative spectra; one for pure CdS thin film and the other for $Cd_{1-x}Zn_xS$ thin film grown at 0.6 M $ZnCl_2$, as all the remaining samples have similar EDX spectra. From the spectra, the presence of Cd, Zn and S is observed in the $Cd_{1-x}Zn_xS$ thin films. The peaks belonging to Si, Sn and O come from the glass/FTO substrate. In addition, carbon peak comes from carbon coating used in sample preparation prior to SEM imaging. As shown in Table 2, as the concentration of $ZnCl_2$ increases, more Zn atoms are incorporated into $Cd_{1-x}Zn_xS$ film and Zn/Cd ratio increases from 0.1 to 0.5 as $ZnCl_2$ concentration in the bath increases from 0.3 to 0.9 M. Similarly, Zn/S ratio increases from 0.1 to 0.4. However, the percentage compositions of Cd and S decrease gradually, when more $ZnCl_2$ is added into the electrolytic

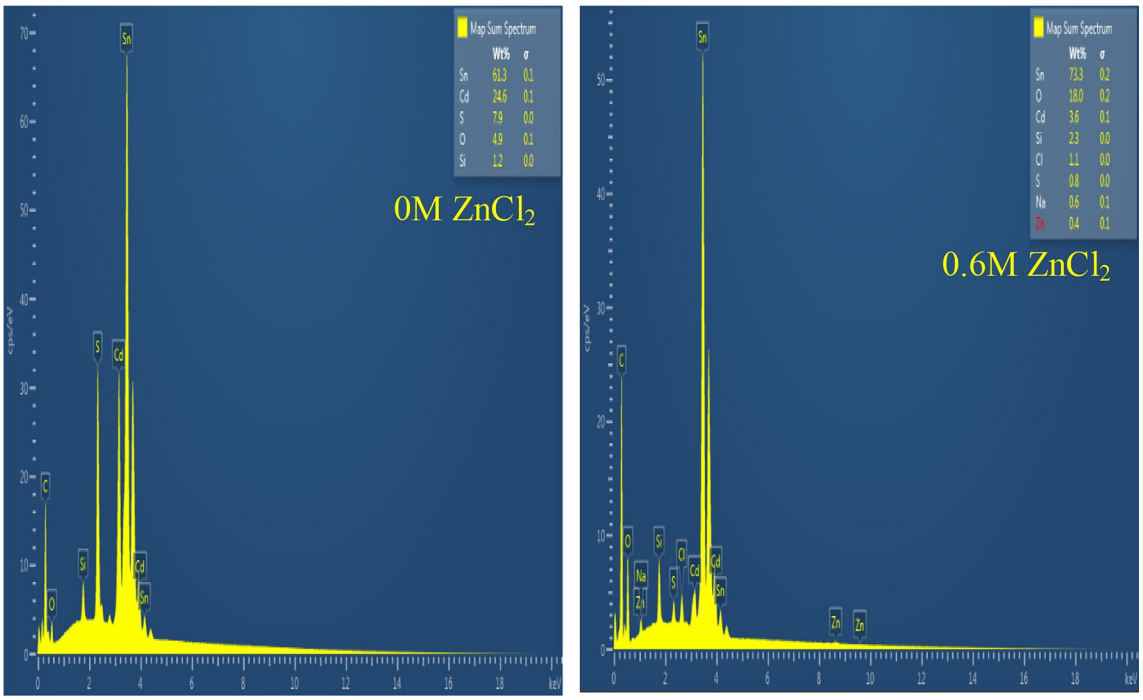

Fig. 4 Representative EDX spectra of annealed CdS and $Cd_{1-x}Zn_xS$ thin films at 0 M and 0.6 M of $ZnCl_2$

Table 2 Atomic composition of Cd, Zn and S in annealed $Cd_{1-x}Zn_xS$ thin films grown at varying zinc chloride concentration

$ZnCl_2$ conc. (M)	Thickness (nm)	Atomic %						Deposition rate (nm/min)	Compound
		Cd	Zn	S	Zn/Cd	Zn/S	S/Cd		
0	437	46.6	–	53.4	–	–	1.1	14.6	CdS
0.3	409	43.9	6.1	50.0	0.1	0.1	1.1	13.5	$Cd_{0.88}Zn_{0.12}S$
0.6	194	39.6	14.7	45.7	0.4	0.3	1.2	6.6	$Cd_{0.73}Zn_{0.27}S$
0.9	151	36.1	19.3	44.6	0.5	0.4	1.2	5.0	$Cd_{0.65}Zn_{0.35}S$

bath. In addition, due to the fact that Zn has high reduction potential as compared to Cd and S, the deposition rate of the bath decreases gradually from 14.6 to 5.0 nm/min as more $ZnCl_2$ is added into the electrolyte. Summary of influence of $ZnCl_2$ concentration on percentage atomic composition of each incorporated atom, deposition rate and thickness of the film is presented in Table 2.

Faraday's equation (Eq. 7) has been used to estimate theoretical thicknesses of all the thin films [27]. The estimated thicknesses of all films at these four different zinc chloride concentrations are in the rage of 437–151 nm. The films were grown for 30 min each, for the purpose of characterization. However, for solar cell application as window/buffer materials, it is enough to grow the films for few minutes. This will reduce the thickness of the films and therefore reduce the absorbance while increasing the transmittance.

$$L = \frac{1}{nFA}\frac{ItM}{d} \tag{7}$$

where L is theoretical thickness of the film in nm, I is the average deposition current in mA/cm^2, recorded at regular interval throughout the deposition period from the computerised potentiostat, M is the molar mass of $Cd_{1-x}Zn_xS$ in grams, t is the deposition time in second, d is the density of $Cd_{1-x}Zn_xS$ in g/cm^3 obtained from the JCPDS reference file used for indexing the deposition films, A is of the surface area thin film in cm^2 measured using a ruler, F is Faraday's constant and n is the number of electrons transferred in the reaction for the formation of 1 mol of CdS or $Cd_xZn_{1-x}S$ based on Eqs. (1–3).

As seen in Table 2, the thicknesses of $Cd_{1-x}Zn_xS$ thin films decrease gradually from 437 nm at 0 M $ZnCl_2$ to 151 nm at 0.9 M $ZnCl_2$. It is known that, thicknesses of thin films are influenced by deposition rates (nm/min), the higher rate of deposition makes the film thicker. However, due to the fact that Zn has high reduction potential as compared to Cd coupled with the high resistivity of ZnS as mentioned earlier, the deposition rate of $Cd_{1-x}Zn_xS$ thin films reduces gradually as more Zn is incorporated into the films and as more $ZnCl_2$ is added into the electrolytic solution. This becomes evident in the drop in deposition current observed during the deposition process, thus leading to decrease in film thickness.

3.3 Raman spectroscopy

Raman spectroscopy measurement has been used to support XRD result of $Cd_{1-x}Zn_xS$ thin films. It is a fast and non-destructive tool for material identification by observing vibrational, rotational, and other low-frequency modes in a material system [28, 33]. It is also a simple way to determine the phase of the material crystalline, noncrystalline or amorphous [34]. As shown in Fig. 5, the Raman

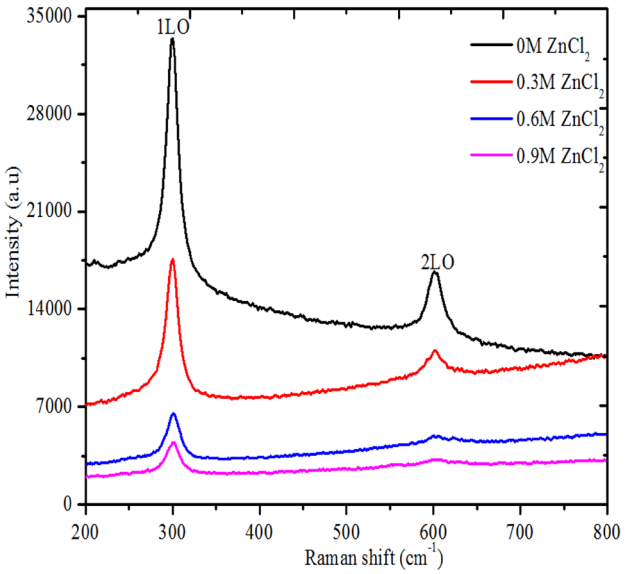

Fig. 5 Raman spectra of annealed $Cd_{1-x}Zn_xS$ thin films grown at different zinc chloride concentrations

spectra of these $Cd_{1-x}Zn_xS$ thin films grown at different $ZnCl_2$ concentrations are compared.

The measurement was taken in the wavenumber range of 200–800 cm^{-1} using Argon laser of wavelength 514 nm. The spectra show two dominant peaks typical of $Cd_{1-x}Zn_xS$, and these dominant peaks belong to the longitudinal optic (LO) vibration mode. They are at wave numbers of 300 cm^{-1} for the first longitudinal optic (1LO) phonon and 600 cm^{-1} for the second longitudinal optic (2LO) phonon. There is no observed shift in the position of the 1LO peaks as $ZnCl_2$ concentration changes. However, for the second longitudinal optic (2LO) vibration mode, there is a continuous shift in the peaks position as $ZnCl_2$ concentration changes. For 0 M $ZnCl_2$ (pure CdS), the peak is at a wave number of 600 cm^{-1} and for 0.3 M, 0.6 M and 0.9 M $ZnCl_2$ it is found to be at 601, 602 and 606 cm^{-1} respectively. Furthermore, the intensity of the Raman peaks decreases as $ZnCl_2$ increases in the electrolytic solution. These decrease in intensity of the peaks come from the incorporation of more Zn atoms in the CdS lattice and associated decrease in film thickness due to reduced deposition rate. At 0 M $ZnCl_2$ (pure CdS), the film has the highest thickness and therefore the highest Raman peak and the smallest Raman peak is recorded when 0.9 M $ZnCl_2$ is added in to the electrolytic solution and in which case the film thickness and deposition rate are lowest. FWHM of the Raman peaks measurement were estimated and increase in FWHM values with increase in $ZnCl_2$ concentration in the electrolytic bath was observed in agreement with the gradual decrease in crystallite size, from XRD result, as more Zn is incorporated into the film. The

highest FWHM value of 22.01 cm^{-1} (1LO) was recorded for the sample grown at 0.9 M $ZnCl_2$ concentration.

3.4 Morphological properties

Figure 6 shows the surface morphology of electrodeposited $Cd_{1-x}Zn_xS$ thin film grown at different $ZnCl_2$ concentrations. The obtained SEM images show that, all films are covered by uniformly distributed and tightly packed grains. However, the surface morphology of the films shows changes as the amount of $ZnCl_2$ added into the electrolytic solution varies. For the sample grown with 0 M $ZnCl_2$ (pure CdS), distinct circular shaped grains of different sizes are observed. But, when more $ZnCl_2$ is added into the bath (i.e. as more Zn is incorporated into the film) the size of the grains become smaller and the shapes gradually change from circular to less distinctly shaped grains. The surface morphologies of $Cd_{1-x}Zn_xS$ thin films are therefore significantly influenced by the amount Zn incorporated into the film.

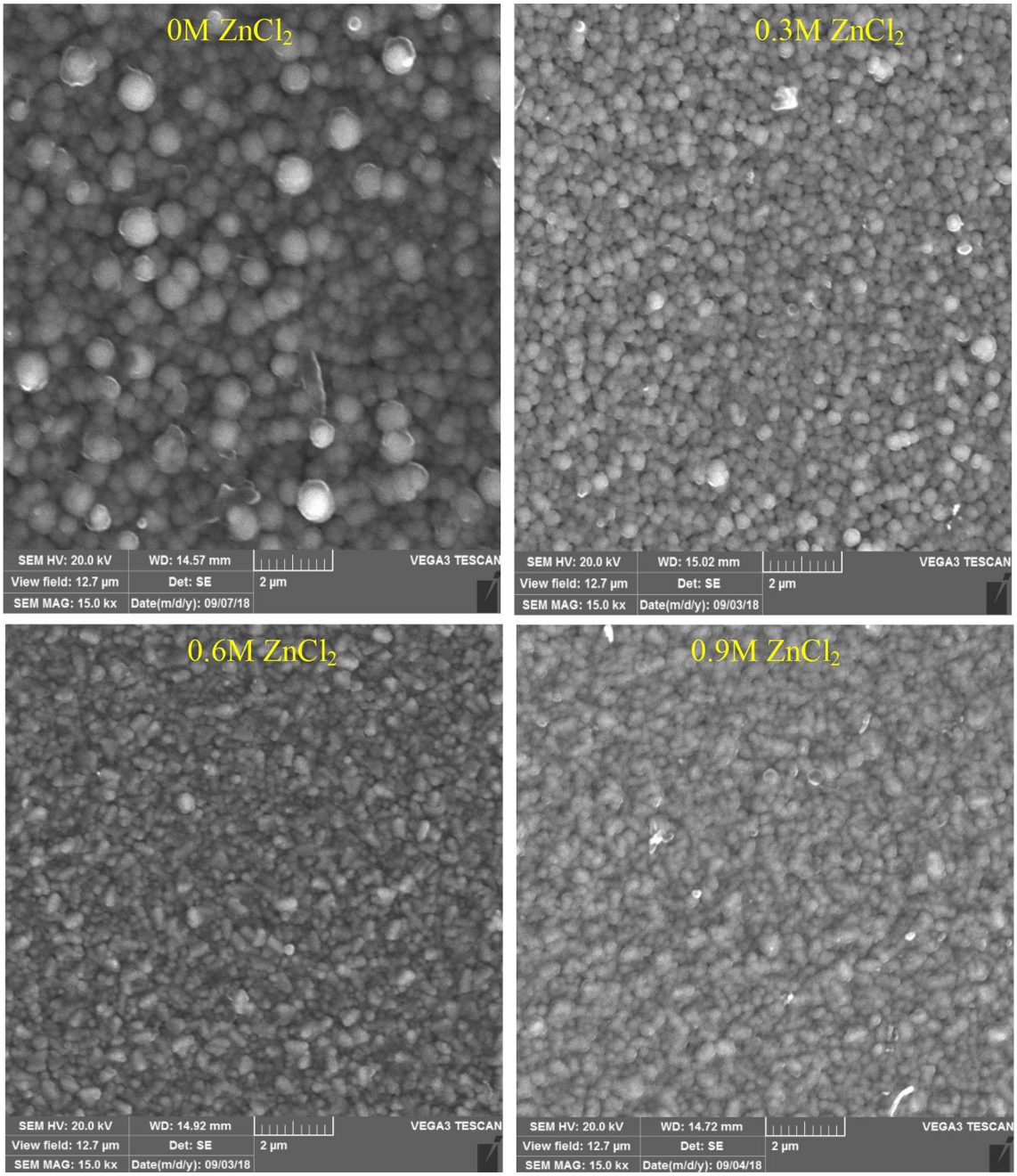

Fig. 6 SEM images of annealed $Cd_{1-x}Zn_xS$ films deposited with different $ZnCl_2$ concentrations

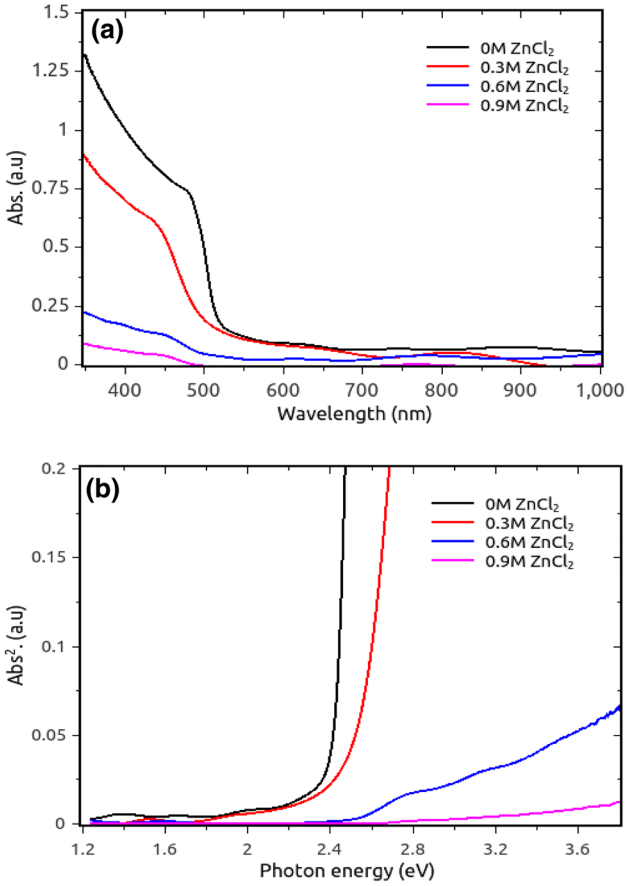

Fig. 7 **a** Absorbance and **b** Abs^2 versus Photon energy band gap graph of annealed $Cd_{1-x}Zn_xS$ thin films grown at different $ZnCl_2$ concentrations

3.5 Optical properties

The optical properties of $Cd_{1-x}Zn_xS$ thin films deposited under different zinc chloride concentrations have been studied using UV–Vis spectroscopy in the wavelength range of 200–1000 nm and the absorbance spectra are shown in Fig. 7a. The spectra show that, pure CdS thin film has high absorbance compared to $Cd_{1-x}Zn_xS$, which is a drawback of CdS thin film as a window/buffer material for solar cell application [35–37]. As Zn is incorporated into the CdS thin film, the absorbance value reduces gradually and the lowest absorbance was recorded at 0.9 M $ZnCl_2$. This decrease in absorbance is attributed to the low thickness of CdZnS as a result of reduction in deposition rate with increasing $ZnCl_2$ concentration in the deposition electrolyte, as already presented in Table 2. This also results in improved transmittance of the CdZnS films as more zinc is incorporated into the material. Another observation about these absorbance spectra is that the absorption edge shifts towards lower photon wavelength as more Zn is incorporated into the film, which suggests enhancement of optical band gap as seen in Fig. 7b.

To determine the energy band gap of $Cd_{1-x}Zn_xS$ thin films, the square of absorbance (Abs^2) as a function of photon energy has been plotted, and the band gap energy estimated by extrapolating the straight line proportion of the graph to the photon energy axis (i.e. to $Abs^2 = 0$). Figures 7b and 8 show that all $Cd_{1-x}Zn_xS$ thin films have higher band gaps than pure CdS thin film and also the absorption edge shifts towards higher energies as Zn-content increases. As

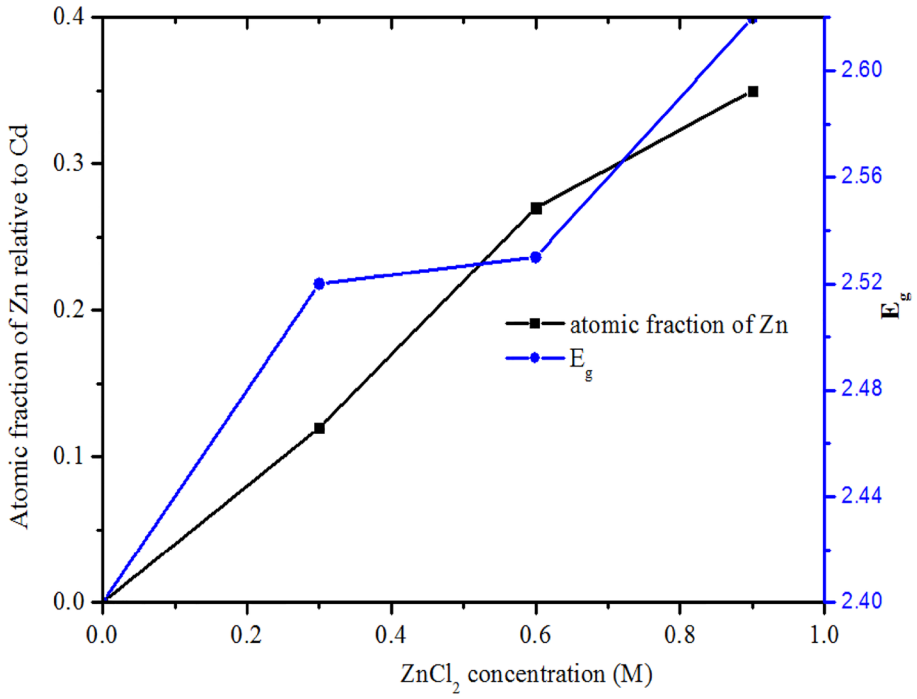

Fig. 8 Atomic composition of Zn and energy band gap (E_g) of annealed $Cd_{1-x}Zn_xS$ thin films versus $ZnCl_2$ concentration

shown in Fig. 8 the energy band gap ranges from 2.40 eV (for pure CdS) to 2.62 eV (with 0.9 M $ZnCl_2$). The increase in concentration of $ZnCl_2$ in the electrolytic solution leads to low deposition rate and incorporation of more Zn into the film and this results in increase in band gap of $Cd_{1-x}Zn_xS$ thin films to 2.52, 2.53 and 2.62 eV for 0.3 M, 0.6 M and 0.9 M $ZnCl_2$ respectively. A large band gap of $Cd_{1-x}Zn_xS$ thin film ($E_g = 2.62$ eV) indicates an improvement in transmittance and decrease in absorbance. This agrees with the transmittance and absorbance results. It is also observed that, the improvement in band gap is almost linear with $ZnCl_2$ concentration increase as shown in Fig. 8.

To measure the non-linear variation of optical band gap (E_g) of $Cd_{1-x}Zn_xS$ thin films over the range of composition '*x*', modified quadratic form of the Vergard's equation has been used as shown in Eq. (8) [5, 38].

$$E_g = E_g^0 + \left(E'_g - E_g^0 - c\right)x + cx^2 \tag{8}$$

Where E_g is experimentally measured band gap of $Cd_{1-x}Zn_xS$ thin films, $E_g^{\,0}$ is energy band gap of CdS (2.42 eV), $E_g^{'}$ is energy band gap of ZnS (3.68 eV), x is Zn composition and c is bowing parameter specifically for alloys.

The bowing parameter was calculated and it is approximately around 1.17, 1.19 and 1.17 for 0.3 M, 0.6 M and 0.9 M $ZnCl_2$ respectively. Therefore, taking the average of these bowing parameters and using Eq. (8), the polynomial fitting of the energy band gap can be expressed as shown in Eq. (9):

$$E_g = 2.42 + 0.26x + 1.18x^2 \tag{9}$$

Approximated value for the bowing parameter of $Cd_{1-x}Zn_xS$ thin films alloys has been reported for films grown by metal organic chemical vapour deposition (c = 0.91) and solution growth technique (c = 0.851) [5, 39]. However, to the best of our knowledge no available report on bowing parameter of $Cd_{1-x}Zn_xS$ grown by the electrodeposition method.

Figure 9 shows the transmittance spectra of the $Cd_{1-x}Zn_xS$ thin films. The transmittance increases with the incorporation of Zn into the film for the same reasons stated earlier in the case of absorbance. Unlike the absorbance spectra, increase in transmittance value is not quite proportional with the incorporation of Zn into the film rather the highest transmittance is recorded at 0.6 M $ZnCl_2$ instead of at 0.9 M $ZnCl_2$. However, the transmittance of the film grown with 0.9 M $ZnCl_2$ is highest in the wavelength range 350–450 nm. This will have an advantage of improving the blue response of solar cell made with this film in comparison with the other films. As discussed in the introduction of this paper, due to its low band gap, CdS window layer has high absorption in the blue region of the solar spectrum, which results in a decrease in current density of the solar cells. However, $Cd_{1-x}Zn_xS$ thin films can resolve this issue by improving the blue response.

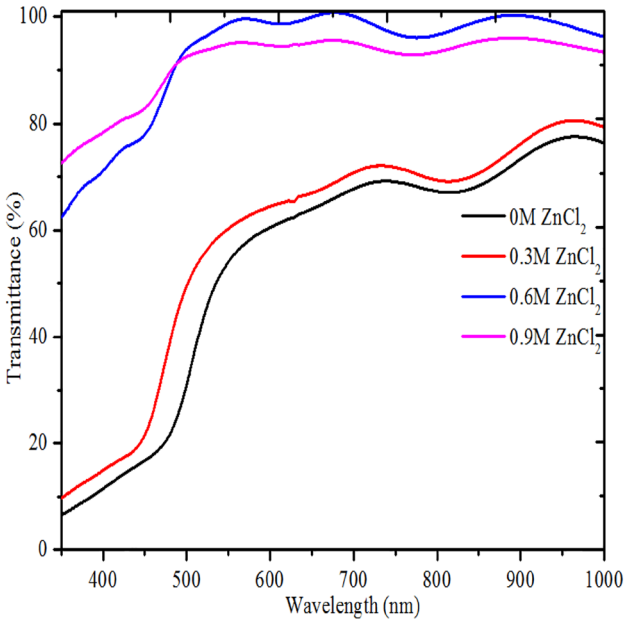

Fig. 9 Transmittance of annealed $Cd_{1-x}Zn_xS$ thin films as a function of different $ZnCl_2$ concentrations

4 Conclusion

Two-electrode electrodeposition and characterization of $Cd_{1-x}Zn_xS$ thin films have been presented. The effect of Zn incorporation into $Cd_{1-x}Zn_xS$ thin films was studied through their structural, compositional, optical and morphological properties. All the films grown with different molar concentrations of $ZnCl_2$ in the deposition electrolyte show polycrystalline hexagonal structure of the material. It is also observed that, as more $ZnCl_2$ is added into the deposition solution, more Zn is incorporated into the films and intensities of the major diffraction and Raman shifts peaks of the $Cd_{1-x}Zn_xS$ films decrease proportionately as a result of low thicknesses of the films arising from reduced deposition rate. All the films are also S-rich. SEM images show uniform coverage of the film surface by $Cd_{1-x}Zn_xS$ grains and the surface morphology changes from distinct circular shaped grains to less distinct grain shapes as more Zn is incorporated into the film. Increase in $ZnCl_2$ in the electrolytic bath results in the production of films with improved transmittance with a significant increase in the energy band gap. Maximum energy band gap of 2.62 eV was obtained with 0.9 M $ZnCl_2$ in the electrolytic solution. Generally, the observed physico-chemical properties of these films suggest

that they can effectively serve as good window/buffer materials in solar cells, with possible improvement in overall solar cell performance compared to the use of CdS.

Acknowledgements The principal author would like to thank National Research Fund, South Africa and Dire Dawa University, Ethiopia for financial support.

Compliance with ethical standards

Conflict of interest The authors declare no conflict of interest.

References

1. S. Azizi, H.R. Dizaji, M.H. Ehsani, Structural and optical properties of $Cd_{1-x}Zn_xS$(x = 0, 0.4, 0.8 and 1) thin films prepared using the precursor obtained from microwave irradiation processes. Optik **127**, 7104 (2016)
2. K. Ghezali, L. Mentar, B. Boudine, A. Azizi, Electrochemical deposition of ZnS thin films and their structural, morphological and optical properties. J. Electroanal. Chem. **794**, 212 (2017)
3. N. Gaewdang, T. Gaewdang, Investigations on chemically deposited $Cd_{1-x}Zn_xS$ thin films with low Zn content. Mater. Lett. **59**, 3577 (2005)
4. Z. Zhou, K. Zhao, F. Huang, Optical properties of $Cd_{1-x}Zn_xS$ thin films for $CuInGaSe_2$ solar cell application. Mater. Res. Bull. **45**, 1537 (2010)
5. G. Kartopu, A.A. Taylor, A.J. Clayton, V. Barrioz, D.A. Lamb, S.J.C. Irvine, $CdCl_2$ treatment related diffusion phenomena in $Cd_{1-x}Zn_xS$/CdTe solar cells. J. Appl. Phys. **115**, 104505 (2014)
6. S.M. Hosseinpour-Mashkani, M. Salavati-Niasari, F. Mohandes, $CuInS_2$ nanostructures: synthesis, characterization, formation mechanism and solar cell applications. J. Ind. Eng. Chem. **20**, 3800–3807 (2014)
7. S.M. Hosseinpour-Mashkani, M. Salavati-Niasari, F. Mohandes, K. Venkateswara-Rao, Mater. Sci. Semicond. Process. **16**, 390–402 (2013)
8. O.I. Oladeji, L. Chow, C.S. Ferekides, V. Viswanathan, Z. Zhao, Metal/CdTe/CdS/$Cd_{1-x}Zn_xS$/TCO/glass: a new CdTe thin film solar cell structure. Solar Energy Mater. Solar Cells **61**, 203 (2000)
9. P. Capper, in *Narrow-gap II-VI Compounds for Optoelectronic and Electromagnetic Applications*, ed. by P. Capper (Chapman and Hall, New York, 1997), p. 211
10. Z.-Q. Qin, F.-J. Zhang, Surface decorated $Cd_xZn_{1-x}S$ cluster with CdS quantum dot as sensitizer for highly photocatalytic efficiency. Appl. Surf. Sci. **285P**, 915 (2013)
11. B.E. McCandless, K.D. Dobson, Processing options for CdTe thin film solar cells. Sol. Energy **77**, 839–856 (2004)
12. S. Stolyarova, M. Weinstein, Y. Nemirovsky, Growth, annealing and thermo-electrical properties of $Cd_{1-x}Zn_xS$ thin films for microbolometers. J. Cryst. Growth **310**, 1674 (2008)
13. L. Wang, W. Wang, M. Shang, W. Yin, S. Sun, L. Zhang, Enhanced photocatalytic hydrogen evolution under visible light over $Cd_{1-x}Zn_xS$ solid solution with cubic zinc blend phase. Int. J. Hydrog. Energy **35**, 19 (2010)
14. H. Kind, H. Yan, B. Messer, M. Law, P. Yang, Nanowire ultraviolet photodetectors and optical switches. Adv. Mater. **14**, 158–160 (2002)
15. O. Amiri, H. Emadi, S.S.M. Hosseinpour-Mashkani, M. Sabet, M.M. Rad, RSC Adv. **4**, 10990 (2014)
16. H.D. Dhaygude, P.P. Chikode, S.K. Shinde, N.S. Shinde, V.J. Fulari, Evaluation of the holographic parameters by electrosynthesized $Cd_xZn_{1-x}S$ (X = 0.3) thin films using double exposure digital holographic interferometry technique. Opt. Laser Technol. **88**, 194 (2017)
17. H. Yao, H. Shen, X. Zhu, J. Jiao, J. Li, W. Wang, Influence of Cd source concentration on photo-current response property of $Cd_xZn_{1-x}S$ film prepared by chemical bath deposition. Ceram. Int. **42**, 2466 (2016)
18. J. Hou, X. Lv, Z. Li, H. Zou, X. Zeng, Controlled synthesis of highly orientation-ordered single crystal $Cd_{1-x}Zn_xS$ nanorod array. J. Alloys Compd. **616**, 97–101 (2014)
19. C. Tian, R. Tang, S. Hu, W. Li, L. Feng, J. Zhang, L. Wu, Comparative studies of CdZnS thin films at low zinc content prepared by vacuum evaporation and CBD. Adv. Mater. Res. **225–226**, 784–788 (2011)
20. K. Hadasa, G. Yellaiah, M. Nagabhushanam, Optical and transport properties of $Cd_{0.8}Zn_{0.2}S$:Cu compounds prepared by modified chemical co-precipitation method. Optik **125**, 6602 (2014)
21. S.M. Thahab, A.H.O. Alkhayat, S.M. Saleh, Influence of substrate type on the structural, optical and electrical properties of $Cd_{1-x}Zn_xS$ MSM thin films prepared by Spray Pyrolysis method. Mater. Sci. Semicond. Process **26**, 49 (2014)
22. A.A. Ziabari, F.E. Ghodsi, Effects of the Cd:Zn:S molar ratio and heat treatment on the optical and photoluminescence properties of nanocrystalline CdZnS thin films. Mater. Sci. Semicond. Process **16**, 1629 (2013)
23. W.S.M. Brooks, S.J.C. Irvine, V. Barrioz, A.J. Clayton, Laser beam induced current measurements of $Cd_{1-x}Zn_xS$/CdTe solar cells. Solar Energy Mater. Solar Cells **101**, 26 (2012)
24. L. Zheng, Y. Lin, L. Li, G. Liang, M. Li, P. Li, Y. He, Structural properties and enhanced bandgap tunability of quaternary CdZnOS epitaxial films grown by pulsed laser deposition. J. Alloys Compd. **650**, 748–752 (2015)
25. M.S. Hossain, M.A. Islam, M.M. Aliyu, P. Chelvanathan, T. RazykovK, K. Sopian, N. Amin, Effect of annealing on the properties of $Zn_xCd_{1-x}S$ thin film growth by RF magnetron Co-sputtering. Energy Procedia **33**, 214–222 (2013)
26. W. Mahmood, N.A. Shah, CdZnS thin films sublimated by closed space using mechanical mixing: a new approach. Opt. Mater. **36**, 1449–1453 (2014)
27. S.Z. Werta, O.K. Echendu, F.B. Dejene, Z.N. Urgessa, J.R. Botha, Temperature-dependent properties of electrochemically grown CdS thin films from acetate precursor. Appl. Phys. A **124**, 576 (2018)
28. O.K. Echendu, S.Z. Werta, F.B. Dejene, K.O. Egbo, Structural, vibrational, optical, morphological and compositional properties of CdS films prepared by a low-cost electrochemical technique. J. Alloys Compd. **778**, 198 (2019)
29. I.M. Dharmadasa, O.K. Echendu, Electrodeposition of electronic materials for applications in macroelectronic and nanotechnology based devices. Encycl. Appl. Electrochem. (2012). https://doi.org/10.1007/978-1-4419-6996-5_37
30. S. Dennison, Dopant and impurity effects in electrodeposited CdS/CdTe thin film for photovoltaic applications. J. Mater. Chem. **4**(1), 41–46 (1994)
31. S. Sain, S.K. Pradhan, Mechanochemical solid state synthesis of $(Cd_{0.8}Zn_{0.2})S$ quantum dots: microstructure and optical characterizations. J. Alloys Compd. **509**, 4178 (2011)
32. S. Saha, S. Sain, A.K. Meikap, S.K. Pradhan, Microstructure characterization and electrical transport of nanocrystalline CdZnS quantum dots. Physica E **66**, 59–66 (2015)
33. G. Selvan, M.P. Abubacker, A.R. Balu, Structural, optical and electrical properties of Cl-doped ternary CdZnS thin films towards optoelectronic applications. Optik **127**, 4946 (2016)

34. R. Kulkarni, A. Pawbake, R. Waykar, A. Jadhawar, H. Borate, R. Aher, A. Bhorde, S. Nair, P. Sharma, S. Jadkar, Single crystal, high band gap CdS thin films grown by RF magnetron sputtering in argon atmosphere for solar cell applications. J. Nano-electron. Phys. **10**, 03005 (2018)
35. A. Ashour, N. El-Kadry, S.A. Mahmoud, On the electrical and optical properties of CdS films thermally deposited by a modified source. Thin Solid Films **269**, 117–120 (1995)
36. X. Wu, High-efficiency polycrystalline CdTe thin-film solar cells. Sol. Energy **77**, 803–814 (2004)
37. I.O. Oladeji, L. Chow, C.S. Ferekides, V. Viswanathan, Z. Zhao, Metal/CdTe/CdS/$Cd_{1-x}Zn_xS$/TCO/glass: a new CdTe thin film solar cell structure. Solar Energy Mater. Solar Cells **61**, 203–211 (2000)
38. W. Xia, J.A. Welt, H. Lin, H.N. Wu, M.H. Ho, C.W. Tang, Fabrication of $Cd_{1-x}Zn_xS$ films with controllable zinc doping using a vapour zinc chloride treatment. Solar Energy Mater. Solar Cells **94**, 2116 (2010)
39. S.V. Borse, S.D. Chavhan, R. Sharma, Growth, structural and optical properties of $Cd_{1-x}Zn_xS$ alloy thin films grown by solution growth technique (SGT). J. Alloys Compd. **436**, 414 (2007)